# The importance of hydrology in routing terrestrial carbon to the atmosphere via global streams and rivers

Shaoda Liu[a,b,1] ⓘ, Catherine Kuhn[c] ⓘ, Giuseppe Amatulli[a,d] ⓘ, Kelly Aho[a] ⓘ, David E. Butman[c,e] ⓘ, George H. Allen[f] ⓘ, Peirong Lin[g,h] ⓘ, Ming Pan[h,i] ⓘ, Dai Yamazaki[j], Craig Brinkerhoff[k], Colin Gleason[k], Xinghui Xia[b] ⓘ, and Peter A. Raymond[a,l]

[a]School of the Environment, Yale University, New Haven, CT 06511; [b]State Key Laboratory of Water Environment Simulation, School of Environment, Beijing Normal University, Beijing, 100875 China; [c]School of Environmental and Forest Science, University of Washington, Seattle, WA 98195; [d]Center for Research Computing, Yale University, New Haven, CT 06511; [e]School of Engineering and Environmental Sciences, University of Washington, Seattle, WA 98195; [f]Department of Geography, Texas A&M University, College Station, TX 77843; [g]Institute of Remote Sensing and Geographic Information System, School of Earth and Space Sciences, Peking University, Beijing, 100871 China; [h]Department of Civil and Environmental Engineering, Princeton University, Princeton, NJ 08544; [i]Center for Western Weather and Water Extremes, Scripps Institution of Oceanography, University of California San Diego, La Jolla, CA 92093; [j]Institute of Industrial Science, The University of Tokyo, Tokyo, 153-8505 Japan; [k]Department of Civil and Environmental Engineering, University of Massachusetts, Amherst, MA 01003; and [l]Department of Earth and Planetary Sciences, Yale University, New Haven, CT 06511

**The magnitude of stream and river carbon dioxide ($CO_2$) emission is affected by seasonal changes in watershed biogeochemistry and hydrology. Global estimates of this flux are, however, uncertain, relying on calculated values for $CO_2$ and lacking spatial accuracy or seasonal variations critical for understanding macroecosystem controls of the flux. Here, we compiled 5,910 direct measurements of fluvial $CO_2$ partial pressure and modeled them against watershed properties to resolve reach-scale monthly variations of the flux. The direct measurements were then combined with seasonally resolved gas transfer velocity and river surface area estimates from a recent global hydrography dataset to constrain the flux at the monthly scale. Globally, fluvial $CO_2$ emission varies between 112 and 209 Tg of carbon per month. The monthly flux varies much more in Arctic and northern temperate rivers than in tropical and southern temperate rivers (coefficient of variation: 46 to 95 vs. 6 to 12%). Annual fluvial $CO_2$ emission to terrestrial gross primary production (GPP) ratio is highly variable across regions, ranging from negligible (<0.2%) to 18%. Nonlinear regressions suggest a saturating increase in GPP and a nonsaturating, steeper increase in fluvial $CO_2$ emission with discharge across regions, which leads to higher percentages of GPP being shunted into rivers for evasion in wetter regions. This highlights the importance of hydrology, in particular water throughput, in routing terrestrial carbon to the atmosphere via the global drainage networks. Our results suggest the need to account for the differential hydrological responses of terrestrial–atmospheric vs. fluvial–atmospheric carbon exchanges in plumbing the terrestrial carbon budget.**

carbon dioxide | greenhouse gases | hydrology | inland waters | biogeochemistry

The Earth's water, carbon, and energy fluxes follow seasonal variations in the Earth's solar radiation and climate variability (1, 2). As an integral part of terrestrial landscapes, streams and rivers receive significant water and carbon inputs from terrestrial and wetland ecosystems, which are further processed along the river to ocean continuum (3). As the largest carbon flux mediated by fluvial systems, carbon dioxide ($CO_2$) emission from stream and river surfaces (4–7) is double the lateral carbon transport to oceans (8), yet its spatial and temporal variations are not fully resolved. Stream and river $CO_2$ evasion changes considerably across space and time due to biogeochemical responses to climatic factors (3), the physics governing the transfer of gas across the water–air interface (9), and seasonal variations in the spatial extent of drainage networks (10, 11). However, seasonal variability of the flux has not been determined at the global scale, limiting our ability to understand controls at the macrosystem level.

The rate at which streams and rivers exchange $CO_2$ with the atmosphere is determined by three factors: dissolved $CO_2$ concentration (often expressed as an equivalent atmospheric partial pressure [$pCO_2$]), water surface gas transfer velocity ($k$), and water surface area. To estimate flux at the monthly scale, all three factors need to be resolved at the same or finer temporal scale(s). To date, existing spatially explicit estimates of riverine $CO_2$ emission at the global scale (4, 12) relied exclusively on $pCO_2$ calculated from carbonate equilibria and historical archives of pH and alkalinity measurements. While these data have reasonable spatial coverage, the carbonate equilibria method is subject to inflated $pCO_2$ estimates due to biased pH measurements (13) and alkalinity contribution from organic acids (14), particularly in low–ionic strength waters. These errors, although reducible within individual datasets (15), are difficult to correct for when scaling globally. This problem has

---

**Significance**

Stream/river carbon dioxide ($CO_2$) emission has significant spatial and seasonal variations critical for understanding its macroecosystem controls and plumbing of the terrestrial carbon budget. We relied on direct fluvial $CO_2$ partial pressure measurements and seasonally varying gas transfer velocity and river network surface area estimates to resolve reach-level seasonal variations of the flux at the global scale. The percentage of terrestrial primary production (GPP) shunted into rivers that ultimately contributes to $CO_2$ evasion increases with discharge across regions, due to a stronger response in fluvial $CO_2$ evasion to discharge than GPP. This highlights the importance of hydrology, in particular water throughput, in terrestrial–fluvial carbon transfers and the need to account for this effect in plumbing the terrestrial carbon budget.

---

significantly undermined calculations and understanding of the flux at the global scale. More importantly, although global estimates of the stream and river surface area and gas transfer velocity at mean annual discharge have been achieved (4, 16), their seasonal extent, a major driver of within-year variability of riverine $CO_2$ flux, has not. This is largely because a temporally resolved reach-scale representation of global river hydrology has not been available until recently (17), and new understandings of aquatic surface area extent and water–air gas transfer rates are necessary to incorporate temporal variability into the riverine $CO_2$ flux estimate.

We compiled a dataset of present-day direct $pCO_2$ measurements in global streams and rivers from the literature. The dataset has 5,910 individual measurements of different months that cover all major freshwater ecoregions of the world (18), despite a small percentage (~0.5%) of measurements from southern temperate rivers (*SI Appendix*, Fig. S1). The dataset further has $pCO_2$ measurements in all months from each freshwater ecoregion (open water months for the polar freshwater ecoregion) except oceanic islands and large river deltas that make up only 0.4% of the global land area (*SI Appendix*, Fig. S1). These observations allowed for robust validation of the study's results. Riverine $pCO_2$ was statistically modeled against a set of watershed properties (*SI Appendix*, Table S1) in order to understand biogeochemical and geophysical controls on $pCO_2$. Predictions of $pCO_2$, $k$, and surface area were based on a new representation of the global river networks (the Global Reach-Level A Priori Discharge Estimates for Surface Water and Ocean Topography [GRADES] river networks) (17), which contains daily discharge estimates at ~3 million individual river reaches over a 35-y period. Monthly $CO_2$ flux estimates were achieved by coupling monthly $pCO_2$ estimates driven by monthly watershed properties to monthly $k$ and surface area estimates driven by the GRADES discharge. Spatial and temporal variability of the flux was finally investigated to demonstrate a strong modulation of the terrestrial (and wetland) carbon routing to the atmosphere via streams and rivers by hydrology.

## Watershed $pCO_2$ Controls

Understanding how stream $pCO_2$ is related to different watershed properties is necessary for improving the mechanistic understanding of the flux and successful modeling of its variability across space and time. Below, we explore broad-scale watershed controls on river $pCO_2$ via linear regressions with delineated watershed properties. Of the 26 watershed properties examined, soil respiration rates (autotrophic, heterotrophic, and total) explain the highest percentages of the $pCO_2$ variability (coefficient of determination or $R^2$ = 0.34 to 0.35) (*SI Appendix*, Fig. S2). Soil organic carbon content (SOC), which measures organic carbon storage in soils, does not correlate with $pCO_2$ ($R^2$ = 0.01), in contrast to earlier studies that use SOC as a major geographical predictor for stream $pCO_2$ (19). Gross primary productivity (GPP), which measures total carbon fixation by terrestrial plants as both biomass increase and plant maintenance respiration, shows a stronger correlation with $pCO_2$ than net primary productivity (NPP), which measures terrestrial carbon fixation as biomass increase ($R^2$ = 0.31 vs. 0.22). Temperature and precipitation are also correlated with $pCO_2$ ($R^2$ = 0.28 and 0.11, respectively), suggesting broad-scale climatic controls on stream $pCO_2$. Wetland areas show a weak correlation with $pCO_2$ at the global scale ($R^2$ = 0.03) despite their importance in tropical lowland rivers (5, 20), suggesting probably local or regional influences in wetland-rich systems.

The fact that soil respiration rates are among the best predictors of river $pCO_2$ highlights close linkages between soil carbon dynamics (in particular, soil $CO_2$ stripping) and watershed

carbon loss through water surface $CO_2$ evasion, widely recognized in headwater streams (21). Watershed properties suggestive of ecosystem carbon storage (e.g., SOC) or net photosynthetic fixation (e.g., NPP) are, however, comparatively less relevant. Considering that direct terrestrial–stream linkages are more significant in small headwater systems (21) or at terrestrial–riverine interfaces in larger systems (6), the strong predictability of stream $pCO_2$ by soil respiration or terrestrial GPP ($R^2$ = 0.31) is also likely caused by broad-scale geographical and seasonal synchronicities between these fluxes (2, 22) and an ensemble of riverine $CO_2$-relevant hydrologic, biogeochemical, and biospheric processes (3) driven by the same climatic factors. Most importantly, temperature and precipitation are two common factors driving terrestrial carbon fluxes and exchanges (1, 2), which underlie the supply of reduced or respired contemporary terrestrial carbon to fluvial systems. Climate factors also strengthen instream processes by enhancing organic carbon metabolism under higher temperatures and/or strengthened hydrologic connectivity (3).

Watershed slope and elevation are negatively correlated with river $pCO_2$ ($R^2$ = 0.33 and 0.19, respectively). Although slope and elevation are partially correlated with each other (e.g., steep terrain is found more often in higher elevations), they point to distinct watershed controls on the $pCO_2$ variability. While high elevations feature colder climates, low terrestrial productivity, and soil respiration rates, the negative effect of watershed slope is also related to rapid release of $CO_2$ from high-gradient, turbulent water columns (19, 23). Considering that $pCO_2$ in flowing waters reflects an equilibrium between the rate of source inputs and surface evasion, the effect of watershed slope is significant as it manifests the physical and geomorphological controls of river $pCO_2$ via surface evasion (9).

## $pCO_2$ Modeling and Seasonal Variability

For a dataset of mixed spatial and temporal observations, it is essential that a model predicts accurate $pCO_2$ across both space and time. Below, we examine how modeling stream $pCO_2$ against watershed properties resolved at the monthly scale vs. modeling them against annual watershed properties differs in predicting the spatial and seasonal variabilities of $pCO_2$. The modeling was done with a random forest (RF) regression model, which accounts for nonlinearities and shows a much stronger predictability than a reduced multilinear (RML) regression model ($R^2$ = 0.77 vs. 0.38) (*SI Appendix*, Figs. S3 and S4). We show that modeling $pCO_2$ against monthly watershed properties yields much stronger predictability for $pCO_2$ than modeling $pCO_2$ against annual values of watershed properties in each individual month ($R^2$ = 0.6 to 0.87 vs. $R^2$ = 0.29 to 0.58) (Fig. 1*A* and *SI Appendix*, Fig. S5). Furthermore, comparing predicted $pCO_2$ against site-level direct seasonal observations suggests that the monthly watershed properties vs. $pCO_2$ approach yield much more reliable seasonal variations than the annual watershed properties vs. the $pCO_2$ approach (Fig. 1*B* and *SI Appendix*, Figs. S6 and S7). This analysis suggests that unavoidable cross-month averaging of watershed predictors and $pCO_2$ by the annual model results in loss of essential seasonal information critical for seasonal variability prediction.

Our estimate shows high consistency with field $pCO_2$ measurements worldwide (*SI Appendix*, Fig. S8*A*). On the whole, $pCO_2$ ranges from below the atmospheric average (380 µatm) to over 10,000 µatm at the reach level (Fig. 2*A*). Spatially, high $pCO_2$ (e.g., >3,000 µatm) is found in hot/humid lowlands, including the tropical Amazon [e.g., reported $pCO_2$ is 3,000 to >12,000 µatm (6)], central Congo [e.g., reported $pCO_2$ is 300 to 17,000 µatm (5)], Southeast Asia, southern subtropical United States, and India. Low $pCO_2$ (e.g., <1,000 µatm) is found in frigid/arid climates where terrestrial inputs and in situ production are likely much weaker (24). Low $pCO_2$ is also found in
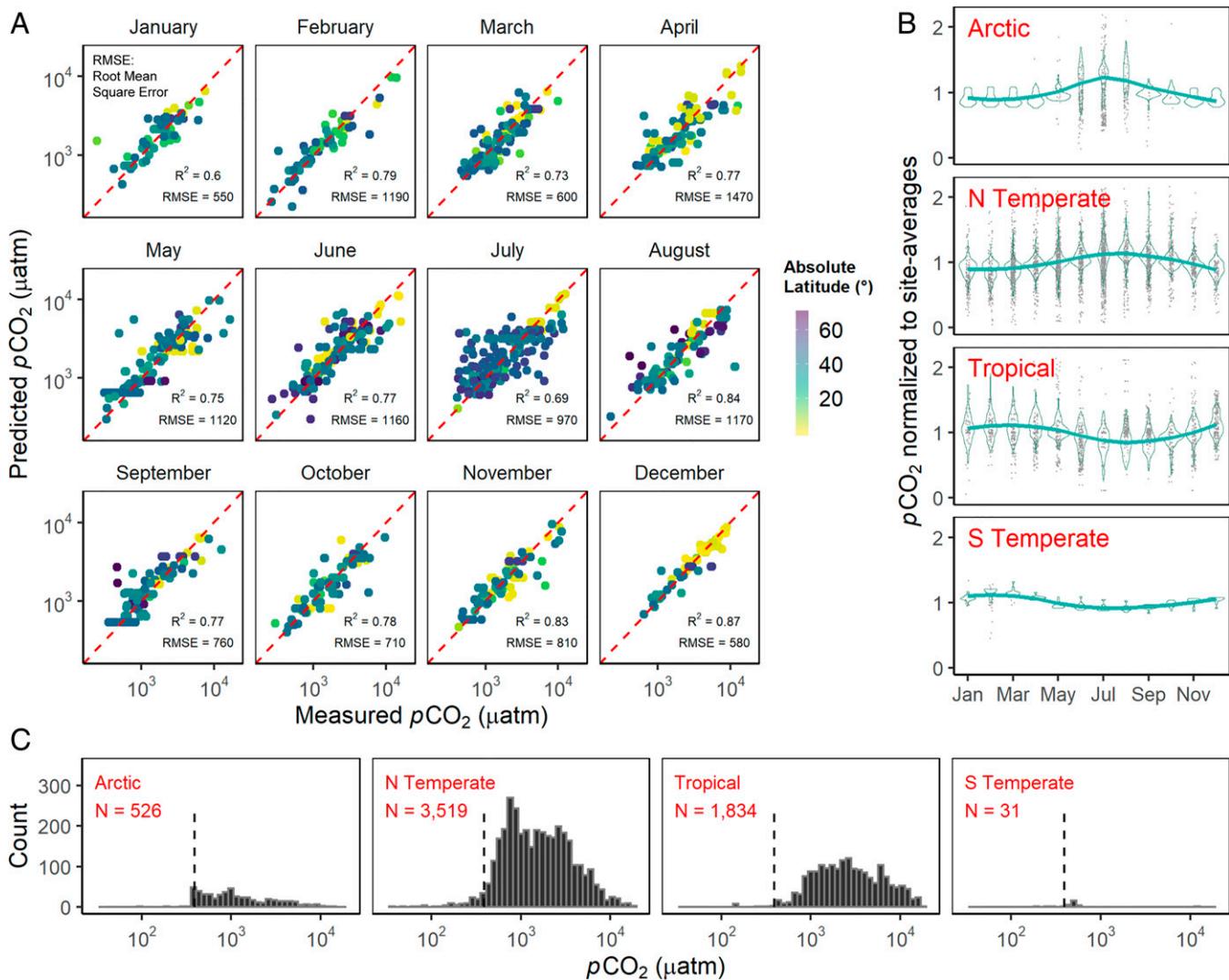
**Fig. 1.** Modeling stream $pCO_2$ against monthly watershed predictors using an RF model. (*A*) Modeled and measured $pCO_2$ values show high correlations ($R^2$ = 0.6 to 0.87) in separate months. (*B*) Predicted $pCO_2$ (normalized to site averages) shows seasonal variations agreeing well with direct observations across climate regions. (*C*) Histograms of the direct $pCO_2$ measurements by climatic regions. Numbers indicate the number of measurements in each climatic zone. Dashed vertical lines indicate the atmospheric $pCO_2$ (∼380 μatm).

elevated, steep-terrain areas where stream $CO_2$ losses due to surface evasion are much stronger (19). As an example, low $pCO_2$ (5th to 95th quantiles: 590 to 1,310 μatm; close to the median of 860 μatm reported in ref. 25) of the upland Tibetan Plateau rivers could be a result of both weak inputs and strong evasion in this area. Across the climate zones, average $pCO_2$ in tropical rivers is 40 to 70% higher than in temperate and Arctic rivers (i.e., 2,560 vs. 1,540 to 1,810 μatm) (Fig. 2*A* and *SI Appendix*, Table S2), which is consistent with the broad-scale geographical $pCO_2$ variability reported by major regional studies (5–7, 26).

Monthly $pCO_2$ variability is greater in Arctic and temperate regions than in tropical regions (coefficient of variation [C.V.]: 8 to 11 vs. 5%) (Fig. 2*B*), in alignment with stronger climatic variability in these areas (i.e., much larger seasonal temperature and precipitation differences) (27). In temperate and Arctic rivers, the highest $pCO_2$ is generally found in the midsummer of each hemisphere (i.e., July and February in the Northern and Southern Hemispheres, respectively), which is 1.2 to 1.4 times the lowest $pCO_2$ in midwinter (Fig. 1*B*). Although in situ plant drawdown is greater during summertime, this is not large enough to drive monthly patterns (28). This seasonal difference

is within the range (one to three times) often reported in temperate streams and rivers (28–30). Tropical regions show higher $pCO_2$ in flooded seasons (Fig. 1*B*), most likely driven by variable hydrologic connectivity to wetlands, a significant $CO_2$ source to tropical rivers (20).

**Gas Transfer Velocity**

Monthly gas transfer velocity was estimated from reach-level slope ($S$) and flow velocity ($V$), which together correspond to the decaying energy dissipation along river networks ($k_{600}$ = 2,841$SV$ + 2.02) (9). We used a gauge-derived discharge to velocity ($Q$-$V$) relationship (i.e., the US Geological Survey equation in ref. 4) to estimate global flow velocities. Comparing predicted flow velocities against those derived from hydrologically routed flows from local and national river networks (*SI Appendix*, Fig. S9*A*) suggests that the low-flow biased $Q$-$V$ relationship derived from the stream gas tracer experiment (9) significantly underestimates flow velocity, particularly for small rivers, which are significant to the global river network surface area (e.g., 0.26 vs. 0.1 m s$^{-1}$ in rivers of <30 m$^3$ s$^{-1}$; these rivers

Liu et al.
The importance of hydrology in routing terrestrial carbon to the atmosphere via global streams and rivers

PNAS | 3 of 9
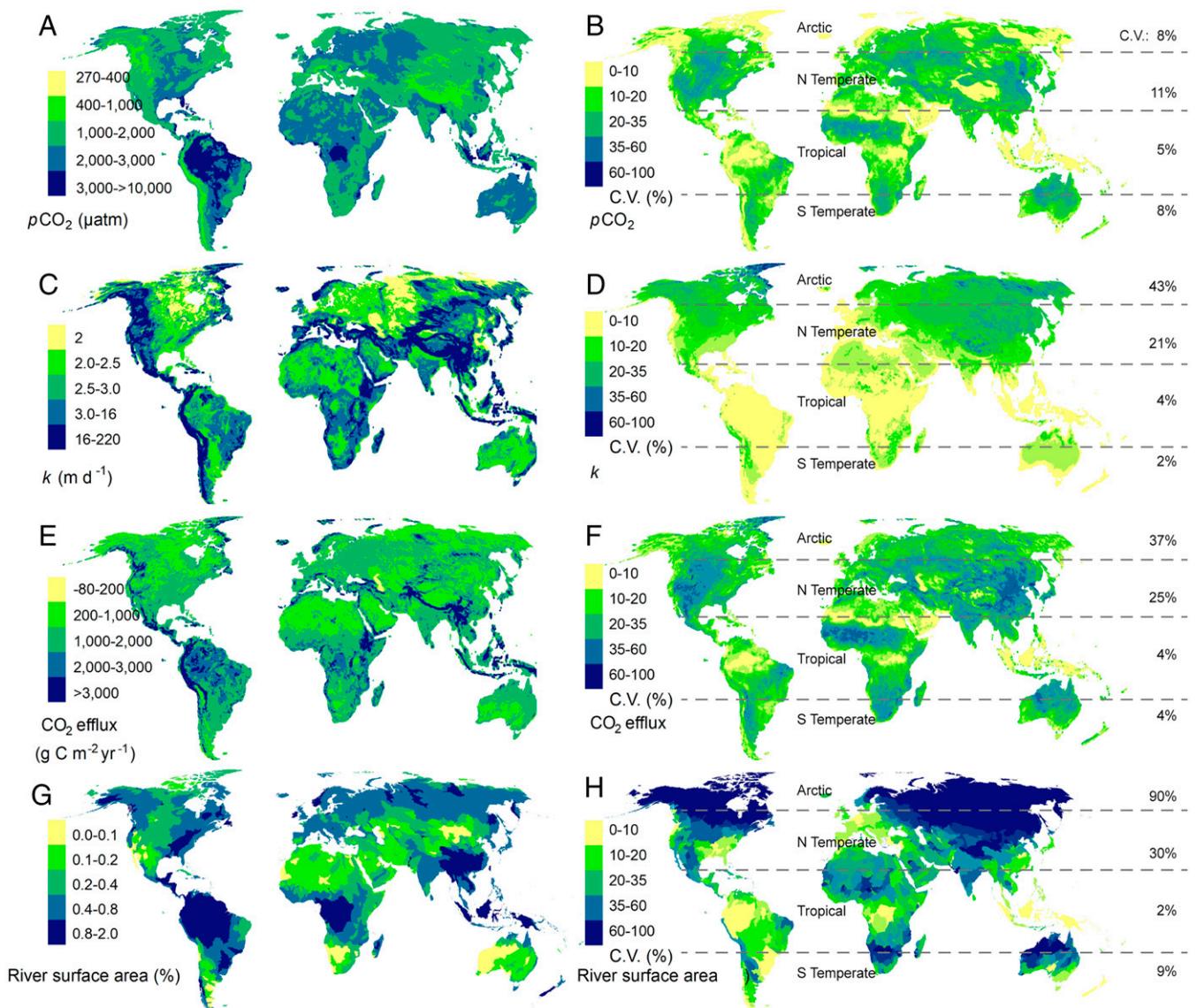https://doi.org/10.1073/pnas.2106322119

**Fig. 2.** Maps showing spatial distribution (*Left*) and monthly variations (expressed as C.V. of monthly values; *Right*) of $pCO_2$ (*A* and *B*), gas transfer velocity (*k*; *C* and *D*), surface $CO_2$ efflux (*E* and *F*), and surface area extent (*G* and *H*) of global streams and rivers. C.V. was calculated from surface area–weighted mean monthly values in each climatic zone (*SI Appendix*, Table S2). Dashed lines (*B*, *D*, *F*, and *H*) indicate latitudes that separate climatic zones. Note that river surface area is shown as a percentage of land area per HydroBASINS Level 04 basin (53).

make up >90% of the 3 million GRADES river reaches). The gauge-derived *Q-V* relationship, however, predicts reliable flow velocity over a broad range of discharge (0.01 to 20,000 m$^3$ s$^{-1}$). In comparison with flow velocity, slope measurements by various digital elevation models (~30-m resolution) are relatively reliable (*SI Appendix*, Fig. S9B) and not expected to cause high uncertainty. Predicted *k* is in good alignment with those reported from regional studies (*SI Appendix*, Fig. S8B).

Bubble-mediated gas exchange has been recently recognized as an important mechanism in high-energy streams (23). This nonlinear mechanism is caused by strong bed friction and significant in mountain streams of shallow water depth and high bed roughness, for which steep terrains act as an integral driver (23). Using a 0.01 (unitless) "mountainous" slope cutoff for streams that have significant bubble-mediated gas exchanges (*SI Appendix*, Fig. S9C), high-slope mountain streams make up 14% of the total GRADES river reaches. For these high-energy systems and affected extrapolated areas, *k* was estimated according to a suggested power law relationship with stream dissipation energy (23). Predicted *k* for

mountain streams is close to that reported in Horgby et al. (19) (16 to 23 vs. 26 m d$^{-1}$) (*SI Appendix*, Table S3).

The highest *k* (e.g., >16 m d$^{-1}$) is found in major elevated regions of the Himalayas, the Rockies, the Andes, the Alps, and eastern Africa, and the lowest *k* (e.g., <3 m d$^{-1}$) is found in major lowlands of low to moderate humidity, including the great plains of North American and western Siberia (Fig. 2*C*). In alignment with decaying energy dissipation rate (eD) along stream order (9), *k* decays significantly with system size (*SI Appendix*, Fig. S9D). Monthly variability in *k* is much stronger in Arctic and northern temperate rivers than in tropical and southern temperate rivers (with C.V. of 21 to 43 vs. 2 to 4%) (Fig. 2*D*) because of the strong annual hydrological variability in northern regions of strong continental climates (27, 31). The highest gas transfer rates are found in midsummer of each hemisphere (*SI Appendix*, Table S2), largely because of the higher late spring/summer flows widely found in many climate types [e.g., flow regime six to eight (31) in monsoon- and ice melt–affected climates] (*SI Appendix*, Fig. S10B).

Liu et al.
The importance of hydrology in routing terrestrial carbon to the
atmosphere via global streams and rivers

## CO₂ Efflux and Seasonal Variability

Predicted $CO_2$ efflux is in general agreement with that reported from regional studies (*SI Appendix*, Fig. S8C). Tropical rivers have much higher $CO_2$ efflux than Arctic and temperate rivers (3,220 vs. 1,750 to 2,280 g C m$^{-2}$ y$^{-1}$) (Figs. 2E and 3). $CO_2$ efflux in temperate rivers is also close to that reported by Butman and Raymond (7) for the northern temperate region (2,060 vs. 2,370 g C m$^{-2}$ y$^{-1}$). Seasonally, similar to $pCO_2$ and $k$, Arctic and northern temperate rivers exhibit much greater monthly variability in $CO_2$ efflux than tropical and southern temperate rivers (C.V.: 25 to 37 vs. 4%, respectively) (Fig. 2F). For instance, the highest monthly average $CO_2$ efflux is twice the lowest average in northern temperate rivers (2,750 vs. 1,360 g C m$^{-2}$ y$^{-1}$), highlighting strong seasonal variability in $CO_2$ flux from these rivers.

## Monthly River Surface Area

Monthly river surface areas were estimated based on a combination of downstream hydraulic geometry (DHG) and at-a-station hydraulic geometry (AHG) and an improved land surface area segregation scheme based on watershed hydrology (*Materials and Methods* and *SI Appendix*, Figs. S10–S12). Total annual surface area of global streams and rivers is 811,000 km², close to the remote sensing–based estimate in Allen and Pavelsky (16) (105%, 773,000 km²) but 30% higher than the raw surface area in Raymond et al. (4) (624,000 km²). Ephemeral area or surface area loss due to temporary drying up of intermittent rivers, estimated using two different methods (*SI Appendix*, Fig. S13), is 4 to 7% of the total river surface area at the global scale and related to watershed runoff. For example, low watershed runoff is responsible for the high ephemeral extent (13 to 16%) found in southern temperate rivers where arid Australian central and western rivers (with watershed runoffs of <50 mm y$^{-1}$) make up a significant portion of the total surface area. Surface area loss due to winter ice coverage is much more variable across climate zones and months than surface area loss due to drying, despite a rudimentary accounting for ice dynamics in this analysis (Fig. 3 and *SI Appendix*, Table S2). Ice coverage is most prevalent between October and April, ranging from 53 to 92% and from 5 to 40% in Arctic and northern temperate basins, respectively. Globally, ice coverage extent ranges from 0 to 27% in different months, lower than the 0 to 56% ice coverage from a recent estimate (32), probably because a rather conservative temperature cutoff ($-4\,°C$) was used for ice coverage initiation. Overall, ice coverage causes a 12% loss to the global river surface area. Accounting for drying up and ice coverage, the monthly area of flowing waters ranges from 500,000 to 854,000 km² and averages 672,000 km² (*SI Appendix*, Table S2), which is 25% higher than the estimate in Raymond et al. (4). The analysis suggests strong cross-month changes in river surface area caused by seasonal variability in global hydrology and ice coverage (Fig. 3). In particular, monthly river surface area is different by a factor of >2.3 in northern temperate watersheds (C.V.: 30%), and that in Arctic regions drops to ~0 in frozen seasons (C.V.: 90%) (Fig. 2H), showing much stronger variability than tropical and southern temperate watersheds (C.V.: 2 to 9%) (Fig. 2H).

## CO₂ Emission and Seasonal Variations

Annual $CO_2$ emission from global streams and rivers amounts to 2.0 ± 0.2 Pg C y$^{-1}$, including corrections for an enhanced release of ~60 Tg C y$^{-1}$ from spring ice melting in northern rivers (*Materials and Methods* and *SI Appendix*, Table S4) and a continued release of ~50 Tg C y$^{-1}$ from dried river channels of intermittent rivers (33). Our estimate is in general agreement with regional estimates from the literature (*SI Appendix*, Table S5). An exception is wetland-dominated tropical lowland
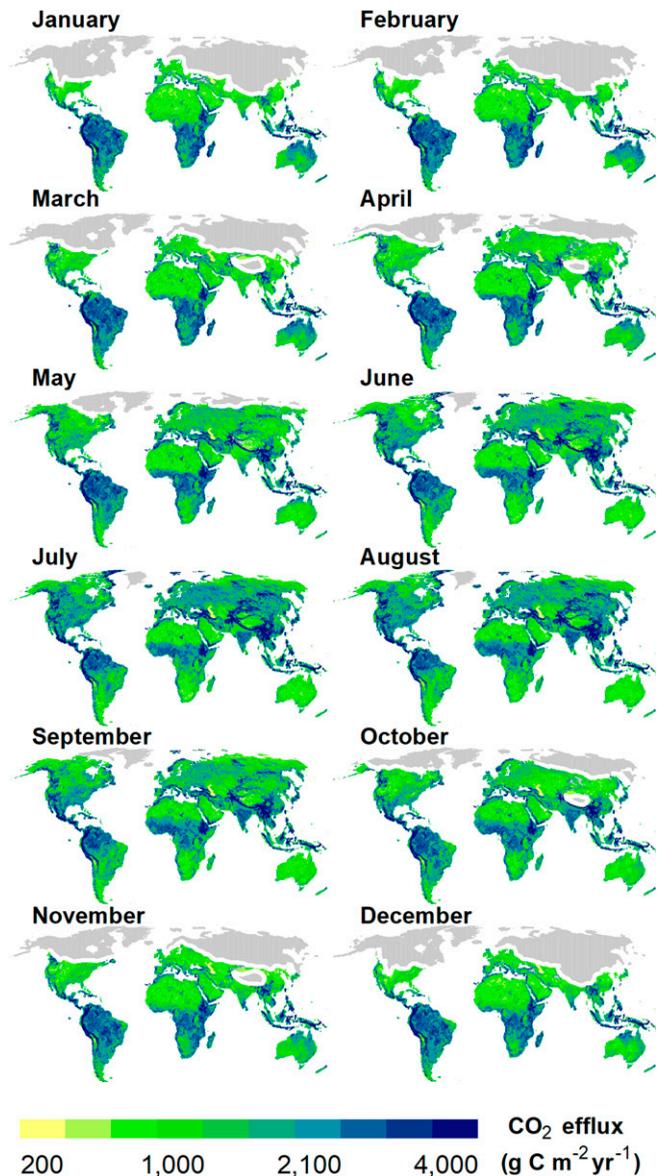


**Fig. 3.** Monthly surface $CO_2$ efflux in global streams and rivers. Ice-covered regions are grayed out for each month.

systems (i.e., the Congo and the Amazon), where our estimate is >20% lower. We suggest that our estimates are conservative because the methods were only able to account for emissions from flowing channels, and those from fringing floodplains or wetlands were not included (6). This becomes evident when comparing our estimates with separate $CO_2$ emission estimates for the Amazonian streams or rivers (floodplains and wetlands excluded) (34), where our estimates are comparable or larger (*SI Appendix*, Table S5). Higher discrepancy between the whole-basin estimates, however, warrants clearly defined boundaries and fully resolved temporal estimates devoted specifically to these systems (20).

Our estimate is slightly higher (~11%) than the earlier estimate of 1.8 Pg C y$^{-1}$, suggesting that the effect of reduced $pCO_2$ from resorting to direct measurements was largely compensated for by higher gas transfer rates and water surface area, particularly from the smallest streams. Across climate regions, tropical rivers are responsible for 57% of the global emission, more than temperate and Arctic regions combined (30 and 13%, respectively), suggesting a dominant role of

Liu et al.
The importance of hydrology in routing terrestrial carbon to the atmosphere via global streams and rivers

PNAS | 5 of 9
https://doi.org/10.1073/pnas.2106322119

tropical rivers in the flux. The climatic zone estimates are in good alignment with earlier estimates from geographical extrapolation of regional surveys. For instance, total riverine $CO_2$ emission for northern temperate rivers was estimated to be 0.54 Pg C $y^{-1}$ (7), in comparison with 0.49 Pg C $y^{-1}$ in this analysis, further corroborating the robustness of the analysis.

Seasonally, $CO_2$ flux varies from 112 to 209 Tg C $mo^{-1}$ (or 1.35 to 2.54 Pg C on an annual basis) (*SI Appendix*, Table S2), suggesting a difference in monthly emissions of a factor of approximately two. The highest emission is found from May to August (203 to 209 Tg C $mo^{-1}$), and the lowest is from November to February (112 to 115 Tg C $mo^{-1}$), corresponding to the seasonality of the Northern Hemisphere where 75% of the land surface is located. Monthly variability is most prominent in Arctic and northern temperate rivers. In northern temperate rivers, the emission varies across months by a factor of 4.5, and in Arctic rivers, the emission drops to ∼0 in frozen seasons and rises until the end of spring freshets (i.e., June) (Fig. 3 and *SI Appendix*, Table S2). The large seasonal variations suggest significant temporal changes in the flux and unreliability of using a single annual estimate (4–7) for the seasonally varying fluvial fluxes (35). While seasonal $pCO_2$ changes are ubiquitous across climate regions (C.V.: 5 to 11%) (Fig. 1*B*), changes in $k$ and water surface area are progressively more significant toward northern colder regions (Fig. 2 *D–H*), for which seasonal variations in watershed hydrology are a key factor (31). It is emphasized that seasonal watershed biogeochemistry and physical constraints imposed by seasonal changes in water surface area and surface water turbulence are important dynamics for seasonal riverine greenhouse gas evasions.

### Terrestrial Carbon Routing to the Atmosphere Modulated by Water Throughput

Stream and river $CO_2$ emissions are driven by terrestrial carbon inputs, either as the stripping and delivery of $CO_2$ from soils (21) or flooded lands (20) or the dissolution/erosion of terrestrial or wetland organic carbon that is later oxidized within drainage networks (3) (*SI Appendix, Terrestrial–Riverine Carbon Transfer Pathways and Terrestrial Carbon Balance* and Fig. S14). Recent work has argued that stream and river $CO_2$ evasion is ultimately balanced by terrestrial GPP (36). Predominant young ages of fluvially evaded $CO_2$ support a strong coupling between the fluvial emission and contemporary terrestrial GPP rather than old terrestrial carbon stocks (37, 38), although exceptions may occur (39). Globally, fluvial $CO_2$ emission makes up ∼1.8% of global GPP (109 Pg C $y^{-1}$) (22) despite a lower river to land surface area ratio (0.5%), reinforcing the concept of streams and rivers as hot spots for terrestrial–atmospheric carbon exchange. Here, we demonstrate that this emission percentage is highly variable, ranging from negligible (<0.2%) to as high as >3.6 to 18% across regions (Fig. 4*A*). Higher percentages are found in both the humid tropics, where the riverine emissions are high, and high latitudes, where terrestrial productivity rates are low and surface soil organic carbon stocks are high (40).

Part of the variability in the percentage of terrestrial GPP routed to the atmosphere via streams and rivers can be explained by water throughput or discharge (Fig. 4*B*). Terrestrial fluxes are rarely looked at through the lens of river discharge, despite discharge being one of the major terms in terrestrial hydrology (41). Here, we find that after we get above a discharge (normalized to watershed area, same below) of ∼100 mm $y^{-1}$ (which occurs on ∼70% of the global watershed surface), there is a clear relationship between discharge and the ratio of stream $CO_2$ evasion to GPP across watersheds (Fig. 4*C*). The relationship is impacted by a number of high-latitude watersheds flanking the Arctic Ocean (Fig. 4*A*) and becomes more linear when the analysis is limited

to watersheds with mean annual temperatures of >8 °C (emission percentage = $0.27 \ln Q + 0.11$, $R^2 = 0.24$) (Fig. 4*C*). The relationships between precipitation and evapotranspiration and this ratio are much weaker ($R^2 = 0.07$ to 0.11) (*SI Appendix*, Fig. S15).

We posit two major mechanisms leading to a greater percentage of terrestrial GPP being shunted to streams and rivers for atmospheric evasion at higher discharge. The first is an increase in the areal extent of drainage networks at higher discharge, demonstrated by a close cross-region correlation between the percentage of river surface area, emission rates, and the emission ratios (Fig. 4 *D* and *E*). Within-watershed studies have also found a higher river surface area during times of greater discharge (10, 42). Stream and river scientists argue that increases in the degree of connectivity between terrestrial and fluvial systems are an important consideration in the transfer of terrestrial constituents to drainage networks (10). We argue that greater connectivity in wetter regions and during wetter months leads to a higher amount and fraction of terrestrial GPP being laterally transported (Fig. 4 *B*, *D*, and *E*).

The second mechanism is the differing responses of fluvial vs. terrestrial fluxes to water throughput. Water is a fundamental constraint on terrestrial plant carbon fluxes. In brief, in order to achieve high rates of $CO_2$ uptake through the stomate (i.e., GPP), terrestrial plants must transpire precipitation water before it enters the river network (43). Plants, however, have a finite need for water to balance GPP due to other limitations on GPP, such as nutrients or light (44, 45). So, we might expect that watersheds with high precipitation have "excess precipitation" that is either stored locally or transported to become river discharge (41, 46). Although quantifying vegetation response to water availability at large spatial scales is difficult, terrestrial studies have demonstrated a response of terrestrial carbon fluxes, including GPP, to the magnitude of precipitation (44, 47). Here, we report a nonlinear relationship between terrestrial GPP and discharge ($\ln GPP = 0.39 \ln Q + 4.7$, $R^2 = 0.66$) (Fig. 4*F*).

The nonlinear relationship suggests a saturation of GPP per increase in discharge (i.e., lower $\Delta GPP$ per $\Delta Q$) at high precipitation, in line with terrestrial studies that demonstrate a lower rain use efficiency for terrestrial plants in wet climates (44, 47). The increase in stream $CO_2$ evasion with discharge, however, does not show a strong saturation and has a steeper response to discharge ($\ln CO_2$ emission rate = $0.67 \ln Q - 1.2$, $R^2 = 0.84$) (Fig. 4*G*). This is in line with stream studies that demonstrate an increase in $CO_2$ evasion and terrestrial carbon export at higher discharge (48, 49). Thus, stream $CO_2$ evasion increases faster than GPP with increasing discharge (slope: 0.67 vs. 0.39), leading to a change in the ratio of fluvial $CO_2$ evasion to terrestrial GPP, with a greater percentage of GPP being laterally delivered to and evaded from drainage networks in wetter watersheds (Fig. 4*B*).

A larger ratio of stream/river $CO_2$ flux to terrestrial GPP in regions of higher discharge provides initial evidence that the global terrestrial water cycle determines in part the relative importance of connectivity between terrestrial and fluvial ecosystems. Recent work has argued that integrating lateral fluxes into terrestrial carbon budgets is important to the estimate of soil respiration (35). These results indicate that improvement can be made to the plumbing of the terrestrial carbon budget if models can account for a differential response of terrestrial–atmosphere vs. terrestrial–drainage network carbon fluxes to water throughput. Furthermore, cold climates with moderate to high watershed discharge and large soil organic carbon stocks might be transporting as much as 5 to 18% of terrestrial GPP (Fig. 4 *A* and *E*) to drainage networks in the form of soil $CO_2$ and organic carbon, highlighting the need for understanding carbon dynamics in these areas.
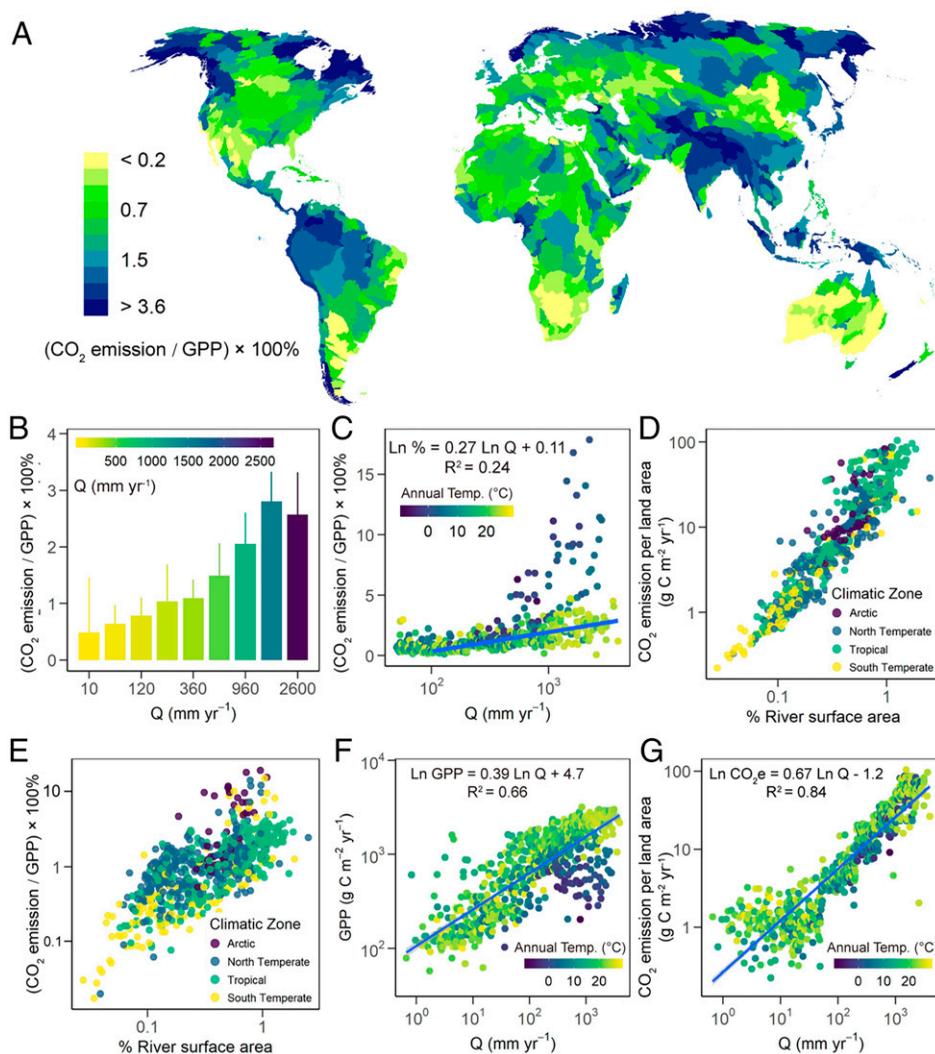
**Fig. 4.** Terrestrial carbon routing to the atmosphere modulated by water throughput. (*A*) Map showing stream $CO_2$ emission as a percentage of terrestrial GPP. (*B*) Stream $CO_2$ emission as a percentage of GPP increases in watersheds of higher water throughput (i.e., discharge). (*C*) The emission percentage increases linearly to logarithmic discharge for watersheds with discharge of >100 mm $y^{-1}$ and annual air temperature of >8 °C. (*D*) Land area normalized stream $CO_2$ emission rate ($CO_2$e) and (*E*) the emission ratio (expressed as a percentage of GPP) scale closely with the river to land area ratio (expressed as percentage of river surface area). *F* and *G* show the power law relationships fitted between GPP and watershed discharge (*F*) and between the emission rate ($CO_2$e) and watershed discharge (*G*), respectively. The relationships suggest a steeper increase to discharge for the emission rate than for GPP (slopes: 0.67 vs. 0.39). In *B*, bars are color coded by watershed discharge levels; error bars indicate SD within each watershed group. Data points in *C*, *F*, and *G* are color coded by mean annual air temperature (degrees Celsius). The map and all relationships are based on HydroBASINS Level 04 (53).

## Materials and Methods

The materials and methods are described in complete detail in *SI Appendix*. The central features are summarized as follows.

To estimate monthly $CO_2$ emissions from global streams and rivers, the three factors ($pCO_2$, $k$, and surface area) determining aquatic $CO_2$ fluxes need to be resolved at the same (i.e., monthly) or finer temporal scale(s). GRADES river networks (17) are a vector-based global drainage network dataset derived from the 90-m Multiple Error-Removed Improved-Terrain Digital Elevation Model (50). GRADES contains ~3 million river reaches and continuous daily discharge estimates at these river reaches over a 35-y period (1979 to 2014). In this analysis, the GRADES river networks were used as the underlying hydrographic infrastructure for global river network $CO_2$ emission estimates. Monthly $pCO_2$, $k$, and surface areas (raw, ephemeral, and ice covered) were estimated at each GRADES river reach. Estimated river $pCO_2$ values were driven by monthly watershed predictors (e.g., soil respiration, GPP, etc.), while $k$ and surface areas were driven by monthly discharge from GRADES.

A dataset containing 5,910 direct fluvial $pCO_2$ measurements was compiled from the literature (Dataset S1). We excluded $pCO_2$ calculated from pH and alkalinity or measurements from open waters, considering that these values are subject to calculation errors (15) or affected by different dynamics than in streams and rivers (30). To predict $pCO_2$ at GRADES river reaches, the $pCO_2$

values were modeled against a set of watershed properties (climatic, geomorphic, and terrestrial carbon-cycling related) using an RF model and an RML regression model (R program, v3.6.2). The RF model outperformed the RML model (as suggested by lower model residuals and less significant bias along the $pCO_2$ range) (*SI Appendix*, Figs. S3 and S4) and was selected for reach-level $pCO_2$ prediction. Furthermore, we demonstrate that modeling individual $pCO_2$ values against monthly watershed properties yields much more reliable seasonal variations than modeling site-average $pCO_2$ against annual watershed properties (*SI Appendix*, Figs. S1 and S5–S7). The RF model was thus established using individual $pCO_2$ values and monthly watershed predictors. Monthly $pCO_2$ values at GRADES river reaches were then estimated using monthly watershed predictors at the river reaches as inputs.

GRADES river reach gas transfer velocities ($k$) were estimated from channel slope ($S$) and flow velocity ($V$; $k_{600} = 2,841SV + 2.02$, $k_{600}$ is the gas transfer velocity normalized to a Schmidt number of 600), which together correspond to the decaying eD along river networks (9). GRADES provides channel slope estimates, which are in high agreement with other products (e.g., National Hydrography Dataset Plus) (*SI Appendix*, Fig. S9B). To scale flow velocity, we coupled monthly discharge from GRADES to a gauge-derived *Q-V* relationship (i.e., $\ln V = 0.12\ln Q - 1.06$) (4), which predicts reliable *V* over a broad range of river discharge (0.01 to 20,000 $m^3\ s^{-1}$) (*SI Appendix*, Fig. S9A).

Liu et al.
The importance of hydrology in routing terrestrial carbon to the atmosphere via global streams and rivers

PNAS | 7 of 9
https://doi.org/10.1073/pnas.2106322119

For streams affected by high bubble-mediated gas exchanges in steep terrains, $k$ was estimated using a reported power law relationship between $k_{600}$ and the eD ($\ln k_{600} = 1.18 \ln eD + 6.43$) (23). A slope cutoff of 0.01 was used to differentiate low- vs. high-energy alpine streams (*SI Appendix*, Fig. S9C).

Monthly river reach widths were estimated by combining DHG and AHG relationships for width (*SI Appendix*, Fig. S12). The DHG relationships were established at the mean annual discharge, which coupled to mean annual discharge from GRADES, were used to scale river widths along the GRADES river networks. AHG relationships, coupled to monthly discharge from GRADES, then allowed for scaling temporal variations in river widths based on widths estimated at the mean annual discharge. AHG width exponents at GRADES river reaches were predicted using a multilinear relationship established between flow characteristics (e.g., C.V. of daily discharge and runoff) and the exponent (*SI Appendix*, Fig. S12 F–I). Reach length was provided by the GRADES river networks. Surface areas were calculated from monthly widths and reach length.

The GRADES river networks start channelization at ~25 km$^2$ (with first stream-order widths of ~2 to 6 m) and miss the smallest streams and rivers. For these streams, $k$ and surface areas were estimated by extrapolating related river hydromorphological or hydraulic characteristics (i.e., width, length, and $k$) according to stream-order scaling laws (51). We used a width of 0.3 m as the cutoff for extrapolation, which is the mean of median headwater stream widths found in a field study (52). $p$CO$_2$ at the extrapolated stream orders was assumed to be the same as that in first-order streams of the GRADES.

It is essential to group land areas with similar flow characteristics together for extrapolation considering that the number of extrapolated stream orders varies spatially and temporally depending on watershed hydrology. An improved hydrology-based segregation scheme was, therefore, employed, which separates the global land surface area into a total of 78 cross-region basins based on watershed runoff levels and flow regimes (i.e., monthly flow distribution) (31) (*SI Appendix*, Figs. S10 and S11). The segregation was also based on the HydroBASINS Level 04 watersheds (53). The cross-region basins were used as the basic land surface unit for drainage network surface area and CO$_2$ emission estimates.

Ephemeral surface areas were corrected for using a nonlinear relationship developed between the mean annual discharge and the ratio of days a stream/river is dry (i.e., zero discharge) within a year (*SI Appendix*, Fig. S13A). Ephemeral surface areas for extrapolated stream orders were corrected for by scaling and extrapolating the estimated ephemeral extents of the GRADES river networks by stream order. Ice-covered river surface areas were corrected for by identifying land surfaces that are under $-4\,°C$ for each month (Fig. 3). CO$_2$ emissions during ice-melt periods were accounted for by applying a reported ice-melt emission ratio (i.e., 0.17) (54) to flowing-water CO$_2$ emissions estimated for each latitudinal band and month (*SI Appendix*, Table S4).

Uncertainties associated with the monthly CO$_2$ emission estimates were evaluated by considering two major sources of error in the current analysis: $p$CO$_2$ error from the RF model and discharge error from GRADES (*SI Appendix*, Fig. S16). A Monte Carlo process was pushed through all steps of the CO$_2$ emission estimation procedures, and uncertainties were calculated as the 1δ deviation of the simulated emission magnitude distributions.

**Data Availability.** The direct $p$CO$_2$ measurement dataset is included as Dataset S1. The monthly $p$CO$_2$, $k$, and CO$_2$ efflux estimates for the GRADES river networks are available at Dryad (https://datadryad.org/stash/dataset/doi:10.5061/dryad.d7wm37pz9). Code related to global stream and river CO$_2$ emission estimates is available at GitHub (https://github.com/lsdeel/globalRiverCO2emission).

1. M. Zhao, S. W. Running, Drought-induced reduction in global terrestrial net primary production from 2000 through 2009. *Science* **329**, 940–943 (2010).
2. B. Bond-Lamberty, A. Thomson, Temperature-associated increases in the global soil respiration record. *Nature* **464**, 579–582 (2010).
3. T. J. Battin et al., Biophysical controls on organic carbon fluxes in fluvial networks. *Nat. Geosci.* **1**, 95–100 (2008).
4. P. A. Raymond et al., Global carbon dioxide emissions from inland waters. *Nature* **503**, 355–359 (2013).
5. A. V. Borges et al., Globally significant greenhouse-gas emissions from African inland waters. *Nat. Geosci.* **8**, 637–642 (2015).
6. J. E. Richey, J. M. Melack, A. K. Aufdenkampe, V. M. Ballester, L. L. Hess, Outgassing from Amazonian rivers and wetlands as a large tropical source of atmospheric CO$_2$. *Nature* **416**, 617–620 (2002).
7. D. Butman, P. A. Raymond, Significant efflux of carbon dioxide from streams and rivers in the United States. *Nat. Geosci.* **4**, 839–842 (2011).
8. J. Cole et al., Plumbing the global carbon cycle: Integrating inland waters into the terrestrial carbon budget. *Ecosystems (N. Y.)* **10**, 172–185 (2007).
9. P. A. Raymond et al., Scaling the gas transfer velocity and hydraulic geometry in streams and small rivers. *Limnol. Oceanogr. Fluids Environ.* **2**, 41–53 (2012).
10. M. A. Zimmer, B. L. McGlynn, Lateral, vertical, and longitudinal source area connectivity drive runoff and carbon export across watershed scales. *Water Resour. Res.* **56**, 1576–1598 (2018).
11. E. Barefoot, T. M. Pavelsky, G. H. Allen, M. A. Zimmer, B. L. McGlynn, Temporally variable stream width and surface area distributions in a headwater catchment. *Water Resour. Res.* **55**, 7166–7181 (2019).
12. R. Lauerwald, G. G. Laruelle, J. Hartmann, P. Ciais, P. A. G. Regnier, Spatial patterns in CO$_2$ evasion from the global river network. *Global Biogeochem. Cycles* **29**, 534–554 (2015).
13. W. Davison, C. Woof, Performance tests for the measurement of pH with glass electrodes in low ionic strength solutions including natural waters. *Anal. Chem.* **57**, 2567–2570 (1985).
14. G. Abril et al., Technical note: Large overestimation of $p$CO$_2$ calculated from pH and alkalinity in acidic, organic-rich freshwaters. *Biogeosciences* **12**, 67–78 (2015).
15. S. Liu, D. E. Butman, P. A. Raymond, Evaluating CO$_2$ calculation error from organic alkalinity and pH measurement error in low ionic strength freshwaters. *Limnol. Oceanogr. Methods* **18**, 606–622 (2020).
16. G. H. Allen, T. M. Pavelsky, Global extent of rivers and streams. *Science* **361**, 585–588 (2018).
17. F. Lin et al., Global reconstruction of naturalized river flows at 2.94 million reaches. *Water Resour. Res.* **55**, 6499–6516 (2019).
18. R. Abell et al., Freshwater ecoregions of the world: A new map of biogeographic units for freshwater biodiversity conservation. *Bioscience* **58**, 403–414 (2008).
19. Å. Horgby et al., Unexpected large evasion fluxes of carbon dioxide from turbulent streams draining the world's mountains. *Nat. Commun.* **10**, 4888 (2019).
20. G. Abril et al., Amazon River carbon dioxide outgassing fuelled by wetlands. *Nature* **505**, 395–398 (2014).
21. M. S. Johnson et al., CO$_2$ efflux from Amazonian headwater streams represents a significant fate for deep soil respiration. *Geophys. Res. Lett.* **35**, L17401 (2008).
22. M. Zhao, F. A. Heinsch, R. R. Nemani, S. W. Running, Improvements of the MODIS terrestrial gross and net primary production global data set. *Remote Sens. Environ.* **95**, 164–176 (2005).
23. A. J. Ulseth et al., Distinct air-water gas exchange regimes in low- and high-energy streams. *Nat. Geosci.* **12**, 259–263 (2019).
24. J. T. Crawford, M. M. Dornblaser, E. H. Stanley, D. W. Clow, R. G. Striegl, Source limitation of carbon gas emissions in high-elevation mountain streams and lakes. *J. Geophys. Res. Biogeosci.* **120**, 952–964 (2015).
25. B. Qu et al., Greenhouse gases emissions in rivers of the Tibetan Plateau. *Sci. Rep.* **7**, 16573 (2017).
26. S. Serikova et al., High riverine CO$_2$ emissions at the permafrost boundary of Western Siberia. *Nat. Geosci.* **11**, 825–829 (2018).
27. S. E. Fick, R. J. Hijmans, WorldClim 2: New 1-km spatial resolution climate surfaces for global land areas. *Int. J. Climatol.* **37**, 4302–4315 (2017).
28. J. T. Crawford, E. H. Stanley, M. M. Dornblaser, R. G. Striegl, CO$_2$ time series patterns in contrasting headwater streams of North America. *Aquat. Sci.* **79**, 473–486 (2017).
29. A. Marescaux, V. Thieu, A. V. Borges, J. Garnier, Seasonal and spatial variability of the partial pressure of carbon dioxide in the human-impacted Seine River in France. *Sci. Rep.* **8**, 13961 (2018).
30. S. Liu et al., Dynamic biogeochemical controls on river $p$CO$_2$ and recent changes under aggravating river impoundment: An example of the subtropical Yangtze River. *Global Biogeochem. Cycles* **30**, 880–897 (2016).
31. A. T. Haines, B. L. Finlayson, T. A. McMahon, A global classification of river regimes. *Appl. Geogr.* **8**, 255–272 (1988).
32. X. Yang, T. M. Pavelsky, G. H. Allen, The past and future of global river ice. *Nature* **577**, 69–73 (2020).
33. P. S. Keller et al., Global CO$_2$ emissions from dry inland waters share common drivers across ecosystems. *Nat. Commun.* **11**, 2126 (2020).
34. J. M. Melack, "Aquatic ecosystems" in *Interactions between Biosphere, Atmosphere and Human Land Use in the Amazon Basin*, L. Nagy, B. R. Forsberg, P. Artaxo, Eds. (Springer, Berlin, Germany, 2016), pp. 119–148.
35. P. Ciais et al., Empirical estimates of regional carbon budgets imply reduced global soil heterotrophic respiration. *Natl. Sci. Rev.* **8**, nwaa145 (2021).
36. P. Ciais et al., Definitions and methods to estimate regional land carbon fluxes for the second phase of the REgional Carbon Cycle Assessment and Processes Project (RECCAP-2). *Geosci. Model Dev. Discuss.* **2020**, 1–46 (2020).

**8 of 9** | **PNAS**
https://doi.org/10.1073/pnas.2106322119

Liu et al.
The importance of hydrology in routing terrestrial carbon to the atmosphere via global streams and rivers

37. A. Campeau *et al.*, Current forest carbon fixation fuels stream $CO_2$ emissions. *Nat. Commun.* **10**, 1876 (2019).

38. E. Mayorga *et al.*, Young organic matter as a source of carbon dioxide outgassing from Amazonian rivers. *Nature* **436**, 538–541 (2005).

39. S. L. McCallister, P. A. del Giorgio, Evidence for the respiration of ancient terrestrial organic C in northern temperate lakes and streams. *Proc. Natl. Acad. Sci. U.S.A.* **109**, 16963–16968 (2012).

40. FAO/IIASA/ISRIC/ISS-CAS/JRC, *Harmonized World Soil Database (Version 1.2)* (FAO and IIASA, Laxenberg, Austria, 2012).

41. S. P. Good, D. Noone, G. Bowen, WATER RESOURCES. Hydrologic connectivity constrains partitioning of global terrestrial water fluxes. *Science* **349**, 175–177 (2015).

42. N. Durighetto, F. Vingiani, L. E. Bertassello, M. Camporese, G. Botter, Intraseasonal drainage network dynamics in a headwater catchment of the Italian Alps. *Water Resour. Res.* **56**, e2019WR022563 (2020).

43. H. G. Jones, Stomatal control of photosynthesis and transpiration. *J. Exp. Bot.* **49**, 387–398 (1998).

44. T. E. Huxman *et al.*, Convergence across biomes to a common rain-use efficiency. *Nature* **429**, 651–654 (2004).

45. J. B. Fisher, G. Badgley, E. Blyth, Global nutrient limitation in terrestrial vegetation. *Global Biogeochem. Cycles* **26**, GB3007 (2012).

46. P. D. Brooks, P. A. Troch, M. Durcik, E. Gallo, M. Schlegel, Quantifying regional scale ecosystem response to changes in precipitation: Not all rain is created equal. *Water Resour. Res.* **47**, W00J08 (2011).

47. M. F. Garbulsky *et al.*, Patterns and controls of the variability of radiation use efficiency and primary productivity across terrestrial ecosystems. *Glob. Ecol. Biogeogr.* **19**, 253–267 (2010).

48. S. Liu, P. A. Raymond, Hydrologic controls on $pCO_2$ and $CO_2$ efflux in US streams and rivers. *Limnol. Oceanogr. Lett.* **3**, 428–435 (2018).

49. P. A. Raymond, J. E. Saiers, W. V. Sobczak, Hydrological and biogeochemical controls on watershed dissolved organic matter transport: Pulse-shunt concept. *Ecology* **97**, 5–16 (2016).

50. D. Yamazaki *et al.*, MERIT Hydro: A high-resolution global hydrography map based on latest topography dataset. *Water Resour. Res.* **55**, 5053–5073 (2019).

51. P. S. Dodds, D. H. Rothman, Unified view of scaling laws for river networks. *Phys. Rev. E Stat. Phys. Plasmas Fluids Relat. Interdiscip. Topics* **59** (5 Pt A), 4865–4877 (1999).

52. G. H. Allen *et al.*, Similarity of stream width distributions across headwater systems. *Nat. Commun.* **9**, 610 (2018).

53. B. Lehner, K. Verdin, A. Jarvis, New global hydrography derived from spaceborne elevation data. *Eos (Wash. D.C.)* **89**, 93–94 (2008).

54. B. A. Denfeld, H. M. Baulch, P. A. del Giorgio, S. E. Hampton, J. Karlsson, A synthesis of carbon dioxide and methane dynamics during the ice-covered period of northern lakes. *Limnol. Oceanogr. Lett.* **3**, 117–131 (2018).

EARTH, ATMOSPHERIC, AND PLANETARY SCIENCES

Liu et al.
The importance of hydrology in routing terrestrial carbon to the atmosphere via global streams and rivers

PNAS | 9 of 9
https://doi.org/10.1073/pnas.2106322119